Experimental and Numerical Investigation on Thermal Performance of Data Center via Fan-wall Free Cooling Technology

Jiang Lan[a], Zujing Zhang[a*], Xing Liang[b], Hongwei Wu[c], Gang Wang[d], Ruiyong Mao[a**]

[a] College of Civil Engineering, Guizhou Provincial Key Laboratory of Rock and Soil Mechanics and Engineering Safety, State Key Laboratory of Public Big Data, Guizhou University, Guiyang, 550025, China

[b] School of Computer Science and Mathematics, Kingston University London, KT1 2EE, United Kingdom

[c] School of Physics, Engineering and Computer Science, University of Hertfordshire, Hatfield, AL10 9AB, United Kingdom

[d] Guizhou nanzhi cloudvalley digital industry development co., ltd, Anshun, 561000, China

[*]Corresponding author: tel: +86 185 2391 9513 email: zjzhang3@gzu.edu.cn.

[**]Corresponding author: tel: +86 139 8505 6628 email: rymao@gzu.edu.cn.

Abstract: With the rapid increase in the scale of data center (DC) construction, DC air conditioning energy consumption has attracted wide attention over the past years. As the DCs are located in the mild climate regions, the air-side free cooling technology that combined with the fan wall air supply demonstrates excellent energy-saving potential. However, there are quite few reports on the environmental thermal response of air conditioning in fan-wall DCs. In this article, the effect of both supply air volume (SAV) and supply air temperature (SAT) on the temperature control performance of the DC are tested through a newly built small fan-wall DC facility. The effect of supply air parameters and the DC's total power (DCTP) are further investigated through numerical simulation. The results show that the server inlet air temperature increases linearly with the SAT and the DCTP, whereas decreases logarithmically with the SAV. The optimal SAV is 0.5 m³/s for a single rack with 2.5 kW when the SAT is 27 °C. Based on the Rack Cooling Index (RCI) evaluation method, an empirical SAV correlation is established and verified against other numerical cases for fan-wall DCs when taking the SAV, the SAT, and the DCTP into account. In the current study, according to the developed model, approximately 34% energy consumption of fans could be saved for fan-wall DCs.

Keywords: Data centers; Fan wall cooling; Thermal environment; Free cooling; Energy saving

Nomenclature

c_p	Specific heat capacity, kJ/ (kg · K)	mr	Maximum recommended
E	Heat flux, W/m²	ma	Maximum allowable
g	Gravitational acceleration vector, m/s²	o	Operating
G_m	Supply air volume, m³/s	s	Supply air
k	Thermal conductivity, W/(m·K)	x	Server inlet air
P	Static pressure, Pa		
Q_{ts}	Data center total power, kW	*Acronyms*	
S	Volumetric heat sources	CACS	Cold aisle containment system
T	Temperature, °C	DC	Data center
u	Velocity vector	DCTP	Data center total power
		HACS	Hot aisle containment system
Greek symbols		PUE	Power usage effectiveness
β	Expansion coefficient	RCI	Rack Cooling Index
v	Effective fluid viscosity	SAT	Supply air temperature
ρ	Density, kg/m³	SAV	Supply air volume
		SIAT	Server inlet air temperature
Subscripts			
a	Static		

1. Introduction

With the rapid development of emerging industries such as computer science and technology and the internet of everything, the data required for storage and processing have risen remarkably. Over the past decade, data centers (DCs) have been evolving rapidly due to a large amount of data in the day-to-day operations of commercial and residential buildings [1, 2]. It is recognized that DCs can consume 40 times more energy than that of typical office buildings [3]. If efficient cooling technologies are not considered in time to prevent heat accumulation, it will induce chip electronic migration, resulting in DC paralysis [4]. It is accounted that the energy consumed by DCs accounts for 1% ~ 2% of the global total electricity consumption in 2020 [5, 6], of which cooling energy consumption accounts for about 30% ~ 50% [7-9].

Free cooling technology is an energy-saving technology that uses free cold sources to cool the DC [10]. The application prospect of free cooling technology is mainly related to outdoor climatic conditions [11]. Nowadays many researchers have studied on the performance of free cold sources, including air and water free-cooling [11, 12]. Compared with water-side free cooling technology, air-side free cooling technology can reduce the heat transfer steps [13], accompanied by more universal and flexible [14]. Oró et al. [15] evaluated the economy of using the direct air-side cooling system in a 1250 kW DC in different areas. Their results showed that the energy consumption of the DC could be reduced by about 15% ~ 22%. Mahdi et al. [16] proposed a combined cooling system, including an air-side economizer, water-side economizer, and air-source heat pump, which could increase the energy efficiency by 16%. Mahdi et al. [17] compared the thermal economy of DCs under air-side economizer, water-side economizer, and combined air and water economizer operating modes. It was found that the combined air and water economizer operating mode could significantly reduce the cooling energy consumption of DCs in all cities except coastal cities. In addition, for most cities, the usage of combined air and water economizer cooling mode could decrease the power usage effectiveness (PUE) of DCs by 10% ~ 12%. Amado et al. [11] proposed a γ index to evaluate the free cooling potential of an area, which was used for 14 cities in Brazil to verify the index. Their results stated that the γ index could well evaluate the free cooling potential. Lee et al. [18] investigated the energy-saving effect of air-side free cooling technology in DCs from multiple meteorological regions by simulation. It was concluded that the cooling potential of air-side free cooling technology could be mainly related to climatic conditions and indoor environment control requirements. Although the air-side free cooling technology has great energy-saving prospects for DCs, not all regions can meet the application conditions of the air-side free cooling technology, this is mainly due to the upper limit of the DC's SAT. ASHRAE recommends that SAT can be controlled between 18 °C and 27 °C [19].

It is recognized that studies on airflow organization optimization in DCs mainly focuses on the air supply of raised floors and row-based air conditioners [20-23]. Zhang et al. [24] found that using a T-shaped floor duct will increase the uniformity of airflow in the DC, compared to traditional rectangular floor ducts. Yuan et al. [25] proposed to use the in-rack cold aisle instead of the traditional raised-floor air distribution to improve the cooling efficiency of DCs. In addition, Yuan et al. [26, 27] improved the airflow in the DC with raised-floor air supply by setting flexible baffles on the front and back doors of the rack. Song et al. [28] proposed to add a deflector in the raised-floor air supply cold aisle could improve the DC environment. Jin et al. [29] studied the optimization of server placement in a rack through experiment and numerical simulation. Their results showed that the servers could have the best thermal performance when they were evenly distributed across the racks. Abbas et al. [30] and Nada et al. [31] analyzed the influence of the air conditioning alignment and interleaving on the cooling efficiency of the row-based air conditioning DC. They concluded that the cooling effect of the air conditioning units' staggered arrangement in racks could be better than that of aligned arrangement. Jin et al. [32] experimentally studied the DC's cooling efficiency under two forms: raised-floor air supply and row-based air conditioning air supply. It was found that the PUE of the DC with row-based air conditioning could decrease by 0.27, compared to the raised-floor supply air.

As a new air supply method for DCs, the fan-wall cooling system is installed with multiple air conditioning

systems on one side wall of the DC. Under the action of the fan, the fresh air from outside passes through the filtering system, the silent segment, the evaporative cooler, and the fan wall system of the air conditioning system in turn, then passes through the punching plate and enters the data room, its working principle is shown in Fig. 1. Cold aisle containment system (CACS) or hot aisle containment system (HACS) is considered to be an important way to avoid hot and cold air mixing in the DC [33, 34]. Unlike traditional DCs such as raised-floor air supply and row-based air conditioning, which normally use the cold aisle containment systems (CACS) [35-37], while fan wall DCs use hot aisle containment systems (HACS) for better adaptability and scalability [38, 39]. Since the fan wall cooling system increases the air supply area, it is easier to combine the system with the air-side free cooling technology [40]. The air-side free cooling technology for fan-wall air supply has been applied to DCs of Huawei and Tencent in Gui-an District of Guizhou Province, China, where the average annual temperature and maximum temperature in summer are 15 °C and 34 °C, respectively, and the annual temperature exceeds 27 °C for less than 600 hours.
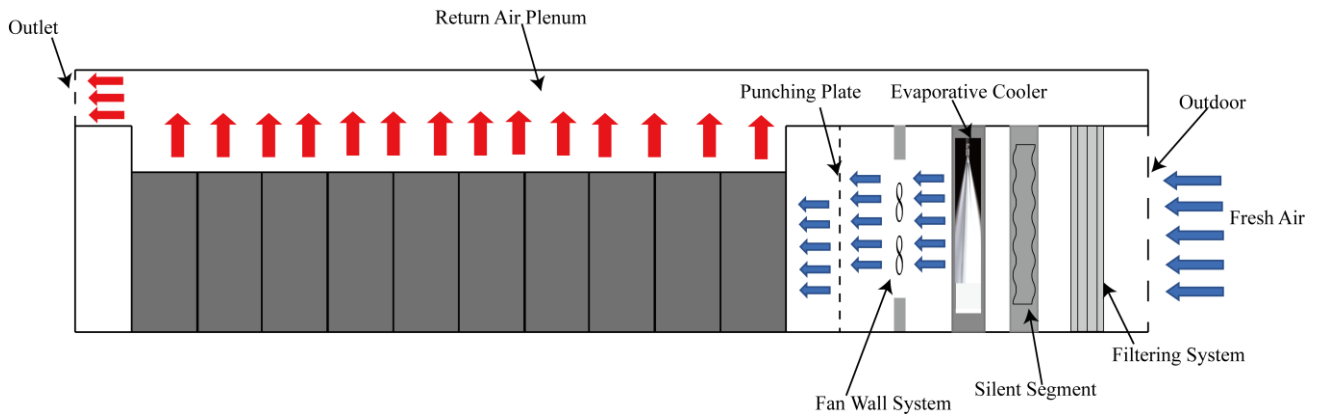

Fig.1. Fan wall DC diagram.

Overall, there are few reports on the environmental thermal response of the air-side free cooling technology for fan-wall DCs. In the current study, the effects of SAT, SAV, and DCTP on the server inlet air temperature (SIAT) were investigated by both experiment and numerical simulation. According to the research results, an empirical method of SAV under different DCTP and SAT was proposed, based on the rack cooling index (RCI) evaluation method. The results could provide a reference for designing and operating the supply air system for fan-wall DCs.

2. Methodology

2.1. Experimental details

2.1.1. Experimental environment and principle

The experimental environment consists of a ventilating room with a size of 3.6 × 3.1 m × 3 m and a cooling room with a size of 3.1 m × 2 m × 3 m, the two rooms are connected by a window with a size of 1.1 m × 0.9 m, as shown in Fig. 2. There are 8 vents with a size of 0.4 m ×0.4 m in the ventilating room, among them, 4 vents are 0.2 m above the ground and the other 4 are 2.2 m above the ground. These vents are connected to air ducts with regulating valves to communicate with the outside. The size of these air ducts is 0.5 m × 0.3 m, the working state of a vent can be controlled by the corresponding switch valve. The cooling room is equipped with a 4.05 kW refrigeration unit, which can control the indoor temperature of the cooling room which can control the indoor temperature range of the cooling room from -20 °C to 50 °C, with the help of an SM102-2 microcomputer controller that linked to 3 PT1000 temperature sensors. Once the indoor temperature range of the cooling room is set, the refrigeration unit will automatically operate when the indoor temperature is above the upper limit value and automatically shut down when the indoor temperature falls below the lower limit value.

Fig. 2. Scene of the experimental environment.

In the current study, a new test rig was built in order to investigate the influence of ventilation parameters on the temperature control performance of the fan-wall DC. The ventilating room is simulated as the data room, the 4 vents located in the lower part of the DC are closed, and the upper 4 vents are used as exhaust vents. There are 4 standard racks with a size of 0.6 m × 0.6 m× 2 m placed in the data room, each rack with 5 simulation servers at a distance of 0.15 m between the two adjacent servers, as shown in Fig. 3(a). The shell of the simulation server is made of 0.7 mm stainless steel, 0.53 m in length, 0.44 m in width, and 0.15 m in height, referring to the dimensions of the standard 4U server. Each server has a heat power of 400 W, simulated by 4 heat tubes of 100 W with fins, as shown in Fig. 3(b). On the air inlet side of each server, there are 3 small fans installed to quickly bring the heat generated by the server into the hot aisle. It has been measured by an anemometer that the air velocity from the small fan is 2 m/s when it is running. The hot aisle is 0.2 m in length and 0.7 m in width, and their ends are closed by a transparent PC board with a thickness of 2 mm. The return air plenum is enclosed with PVC plastic plates. There are 4 variable frequency fans with a diameter of 0.6 m installed at the connection window of the two rooms to simulate the fan wall system, as illustrated in Fig. 3(c). The SAV of these fans can be controlled from 0 to 3.5 m^3/s by an inverter (model: 4.0G2-220V), as demonstrated in Fig. 3(d). More detailed dimension information of the test rig is listed in Table 1.

| (a) Rack | (b) Heat source | (c) Variable frequency fan | (d) Inverter |

Fig. 3. Experimental platform of the fan-wall cooling DC.

The principle of the experimental process can be seen in Fig. 4. Fresh air from the outside enters the cooling room through the half-opening door, then the air will be cooled by a refrigeration unit. Afterwards, the cold air will enter the data room with the assistance of 4 variable frequency fans. Inside the data room, the cold air is sucked into servers by small fans, flows through the heat tubes, then becomes hot air, flowing into the hot aisle and the return air

plenum in turn. Finally, the hot air will be discharged from 4 vents in the return air plenum to the outside.

Table 1

Geometric dimension of DC test model.

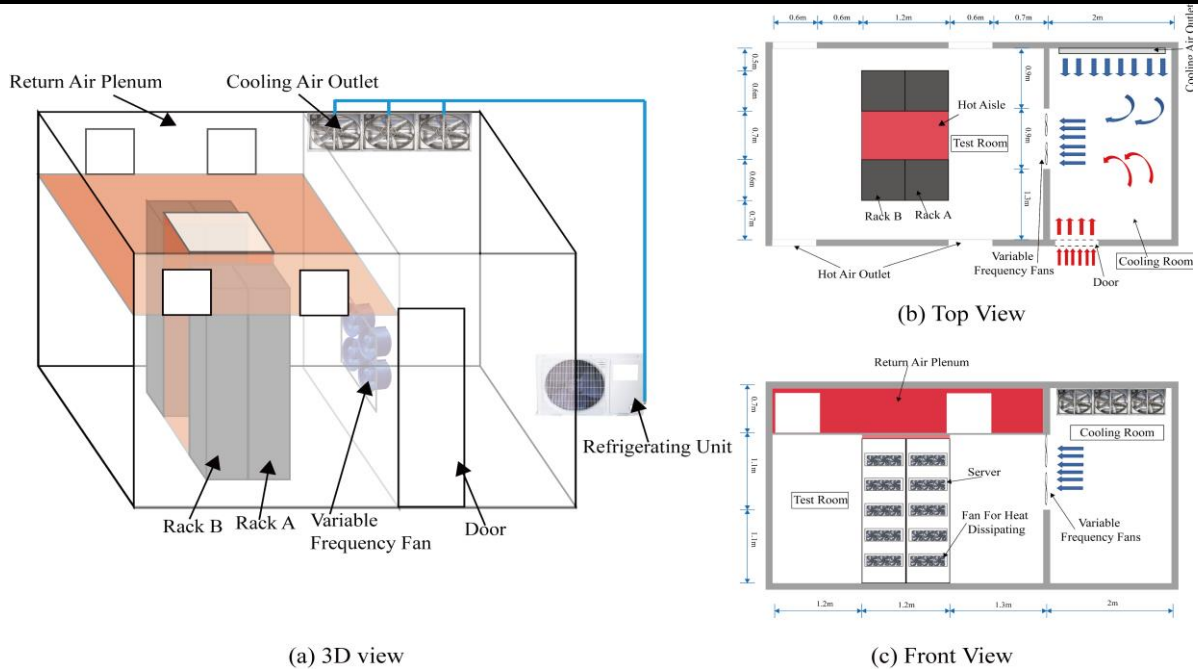| Items	Dimension
Cooling room	3.1 m (L) × 2 m (W) × 3 m (H)
Ventilating room	3.6 m (L) × 3.1 m (W) × 3 m (H)
Hot aisle	1.2 m (L) × 0.7 m (W) × 2.1 m (H)
Connection window	1.1 m (L) ×0.9 m (W)
Return air plenum	3.6 m (L) × 3.1 m (W) × 0.9 m (H)
Variable frequency fan	0.3 m
Rack	0.6 m (L) × 0.6 m (W) × 2 m (H)
Shell of the server	0.53 m (L) ×0.44 m (W) ×0.15 m (H)
Small fan of the server	0.12 m (L) ×0.12 m (W) ×0.038 m (H)

(a) 3D view

(b) Top View

(c) Front View

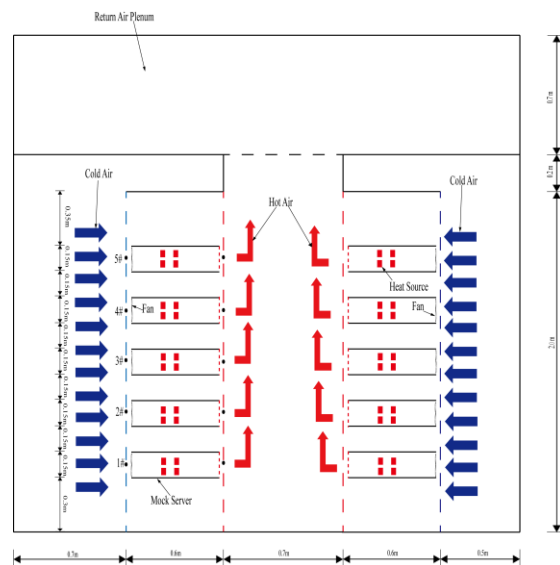**Fig. 4. Layout of the DC.**

2.1.2. Data collection

Fig. 5. Layout of the air temperature measuring points.

Air temperature at the air inlet of servers is a significant indicator to evaluate the thermal environment of the DC. In the current work, five temperature measuring points are arranged at the air inlet and outlet of racks A and B, which correspond to the center of the air inlet and outlet of each server, respectively, 0.38, 0.68, 0.98, 1.28 and 1.58 m above the ground, as seen in Fig. 5. Air temperature of these measuring points will be measured by the PT100 thermocouple, which has a measurement range of -50 °C ~ 200 °C with an accuracy of less than 0.1 °C, then they will be recorded by a MIK-6000 F paperless recorder. The temperature and the velocity of the air supply are measured by a PT100 thermocouple and a FLUKE-925 handheld anemometer with a range of 0.40 ~ 25.00 m/s and an accuracy of ± 2%, respectively. The wind speed of the pipeline is measured by a wind speed transmitter, which has a measuring range of 0 ~ 30 m/s, an accuracy of ± 2% and a resolution of 0.1 m/s.

2.1.3. Experimental cases

The experiment mainly focuses on the influence of the SAT and SAV on the temperature control performance of the fan-wall DC. In the current study, the influence of the ventilation humidity was not considered since the limitation of the experimental conditions. The SAT ranges from 18 °C to 27 °C in the experiment, referring to the recommended value of SIAT in ASHRAE [19]. According to Xiong et al. [41], the minimum supply of the air required for a server is 0.044 m^3/s, which means that the minimum SAV for the experimental DC is 0.88 m^3/s. To facilitate control of the experimental process, the lower limit of the SAV for the DC is 1 m^3/s, and the upper limit is 3 m^3/s, due to the limitation of the working capacity of the variable frequency fans. The experimental cases are shown in Table 2.

Table 2

Experimental case design.

Case	1	2	3	4	5	6
SAT (°C)	21	21	21	18	24	27
SAV (m^3/s)	1	2	3	1	1	1

2.1.4. Experimental procedure

The main experimental steps are as follows:

(1) Set 1 minute as the save time for the paperless recorder and ensure the reliability of the monitor system.

(2) Turn on the refrigeration unit, and set the upper limit of the microcomputer controller to 21.1 °C and the lower limit to 20.9 °C, considering experimental case 1.

(3) Properly open the door of the cooling room to compensate for fresh air.

(4) Run the variable frequency fans and adjust the wind speed to 1 m/s through the frequency converter with the assistance of the handheld anemometer. Meanwhile, the pipe wind speed is maintained at around 6.5 m/s ~ 6.8 m/s, and monitored by the pipeline wind speed transmitter.

(5) Run the variable frequency fans and adjust the wind speed to 1 m/s through the frequency converter with the help of the handheld anemometer.

(6) Power on the heating tubes and server small fans for 1.5 h.

(7) Switch off the power of the heating tubes, small fans, frequency converter, and refrigeration unit in turn after the test case is over.

(8) Repeat the above experimental steps and change the ventilation parameters according to experimental cases listed in Table 2. After the experimental environment returns to normal temperature, until all experimental cases are completed.

(9) Analyze the temperature data which has been recorded by the paperless recorder.

2.2. Computational details

2.2.1. Computational model and mesh

A computational model is established against the experimental DC by ANSYS ICEM. The space of the cooling room is ignored because it hardly affects the thermal environment of the DC. In the computational model, the dimensions of the DC, air inlet, air outlets, racks, hot aisle, and the return air plenum, etc., are consistent with that in the experiment. The area of the small fans for each server is simplified to a rectangle surface with a size of 0.36 m in length and 0.12 m in width. To facilitate the division of the structured mesh, the shape of each heat tube is simplified into a cuboid, with 0.3 m in length, 0.025 m in width and 0.025 m in height. There are 6 heat tubes placed inside each server, which are evenly distributed in two rows inside the server. The distance between the two adjacent heat tubes is 0.1 m in horizontal and 0.03 m in height. To reduce the error caused by the high temperature and velocity gradient near the wall, and to better capture the flow field characteristics during the calculation process, the mesh on the surfaces of heat sources, servers, internal fans, etc., is encrypted. The maximum grid sizes in different zones are shown in Table 3. The computational model of the fan-wall DC is shown in Fig. 6.

Table 3

Maximum grid size in different areas.

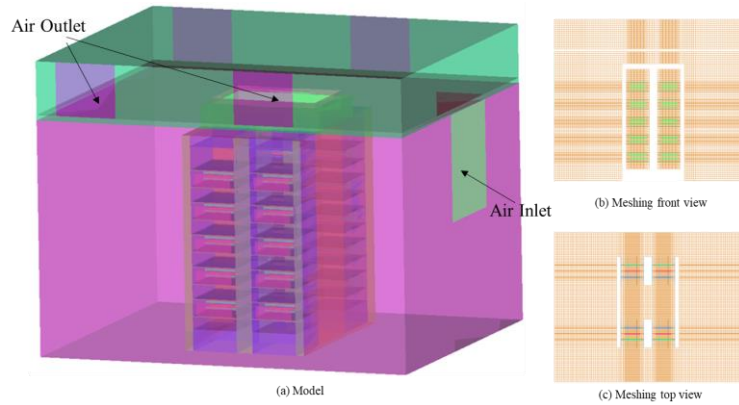| Zones	Cold aisle, hot aisle and return air plenum	Rack surface	Server surface	Internal fan surface	heat source surface
Maximum grid size/(mm)	0.057	0.04	0.03	0.023	0.005

Fig. 6. Computational model of fan wall DC: (a) model; (b) meshing front view; (c) meshing top view.
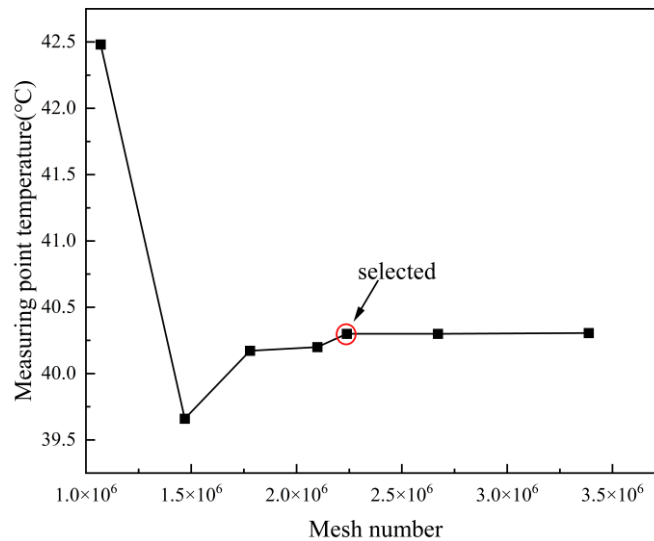

Fig. 7. Variation of air temperature under different grids.

In the current work, a mesh independence study was carried out, seven different grids are selected. The numerical results of numerical case 3 are selected for the purpose of comparison. Fig. 7 plots the variation of air temperature at the measuring point 0.68 m above the ground on the air outlet side of rack A under different grids. It can be found from Fig. 7 that the temperature value of the measuring point oscillates greatly when the number of meshes is below 2238249, and after that, continuing to increase the mesh number has little effect on the temperature value. Therefore, the grid model with a mesh number of 2238249 and mesh quality of 0.85 is selected for the current numerical analysis, considering the saving of computer resources and accuracy.

2.2.2. Turbulence model

It is noted that proper selection of turbulence modeling not only improves the accuracy of numerical results but also saves calculation time. Currently, turbulence models including the Realizable k–ε turbulence model [23,33], Standard k-ε turbulence model [28,42] and RNG k-e model [43] have been used to numerically analyze the thermal performance of DCs. In the current work, the Standard k-ε turbulence model is selected since it can meet the simulation requirements of DCs in most cases [44]. The standard wall function is selected to solve the velocity and shear stress near the wall.

The following assumptions are considered: 1) the air is regarded as an incompressible fluid; 2) the airflow is stable; and 3) the Boussinesq approximation simulates the buoyancy of natural convection.

The continuity, momentum, and energy equations of airflow are as follows:

$$\nabla \cdot u = 0 \tag{1}$$

$$\frac{\partial u}{\partial t} + u \cdot \nabla u = \nabla \cdot (\nu \nabla u) - \frac{1}{\rho}\nabla p + \beta(T_a - T_0)g \tag{2}$$

$$\rho c_p \left[\frac{\partial T}{\partial t} + (u \cdot \nabla)T_a \right] = \nabla \cdot (k \nabla T) + S \tag{3}$$

where u is the velocity vector; p is the static pressure; T_a is the static temperature; β is the coefficient of thermal expansion; T_o is the operating temperature; g is the gravity acceleration (9.81 m^2/s); v and k are the effective fluid viscosity and thermal conductivity; ρ is density; c_p is the specific heat capacity; S is the volume heat source.

2.2.3. Numerical cases

The influence of DCTP on the temperature control performance of the DC will be numerically analyzed. In addition, considering that the SAT of 27 °C is the upper value for DCs, it is of great significance to further explore the SAV that meets the temperature control requirements of a fan-wall DC under this condition. Referring to experimental results of an actual DC rack power in Jin et al. [29], the lower and upper limit power of a rack is set to 1 kW and 3 kW, respectively. That is the DCTP ranges from 4 kW to 12 kW. Considering that the current average rack power of DCs is about 2.5 kW, the impact of SAV on the thermal environment of the DC is further explored when the DCTP is 10 kW and the SAT is 27 °C. Parameters of the DCTP, SAT, and SAV for numerical cases are listed in Table 4.

Table 4

Numerical case design.

Case	1	2	3	4	5	6	7	8	9	10
DCTP (kW)	4	6	8	10	12	10	10	10	10	10
SAT (°C)	21	21	21	21	21	27	27	27	27	27
SAV (m^3/s)	1	1	1	1	1	1	1.5	2	2.5	3

2.2.4. Boundary Condition and Solution Setting

The air inlet is set as a velocity inlet, and the values of temperature and speed are assigned according to the ventilation parameters in the numerical cases listed in Table 4. The air outlet is set as a pressure outlet with 0 Pa. The

fan surface of each server is set as a fan boundary, with a pressure of 2.1 Pa, which is calculated by the Bernoulli equation. The surface of each heat tube inside the server is set as a wall boundary with an area of 0.03 m^2. When a heat tube is considered as a heat source, its heat power is 100 W, thus, the heat flux value of the heat tube surface is 3333 W/m^2. If not, it is considered as an insulating surface with a heat flux of 0 W/m^2. Which depends on whether it works or not. For example, when the server power is 300 W, the heat flux for the selected three heat tubes is 3333 W/m^2, while for the other three heat tubes is 0 W/m^2. The remaining walls are adiabatic boundary conditions without slip.

Pressure-based segregated algorithm with SIMPLE pressure-velocity coupling is adopted for the current simulation. The second-order upwind scheme is applied to ensure the numerical accuracy. Default values for relaxation factors are used in the current work. Convergence criteria of velocity, continuity, energy and dissipation rate are set to $1 \times 10^{-3}, 1 \times 10^{-3}, 1 \times 10^{-6}$ and 1×10^{-3}, respectively. It normally takes approximately 2 hours for each numerical case to get converged with a computer of AMD Ryzen 3960x processor.

2.3. Model validation

The reliability of the numerical model is verified by the results of experimental case 1, case 3 and case 6, respectively. Fig. 8 compares the experimental and numerical SIAT at the measuring points of racks A and B under the three different cases. It needs to be noted here that the measuring points A1#, A2#, A3#, A4# and A5# are used to measure the SIAT of rack A, and measuring points B1#, B2#, B3#, B4# and B5# are used to measure the SIAT of rack B, respectively. The height of each measuring point on a single rack is consistent with that in Fig. 5.
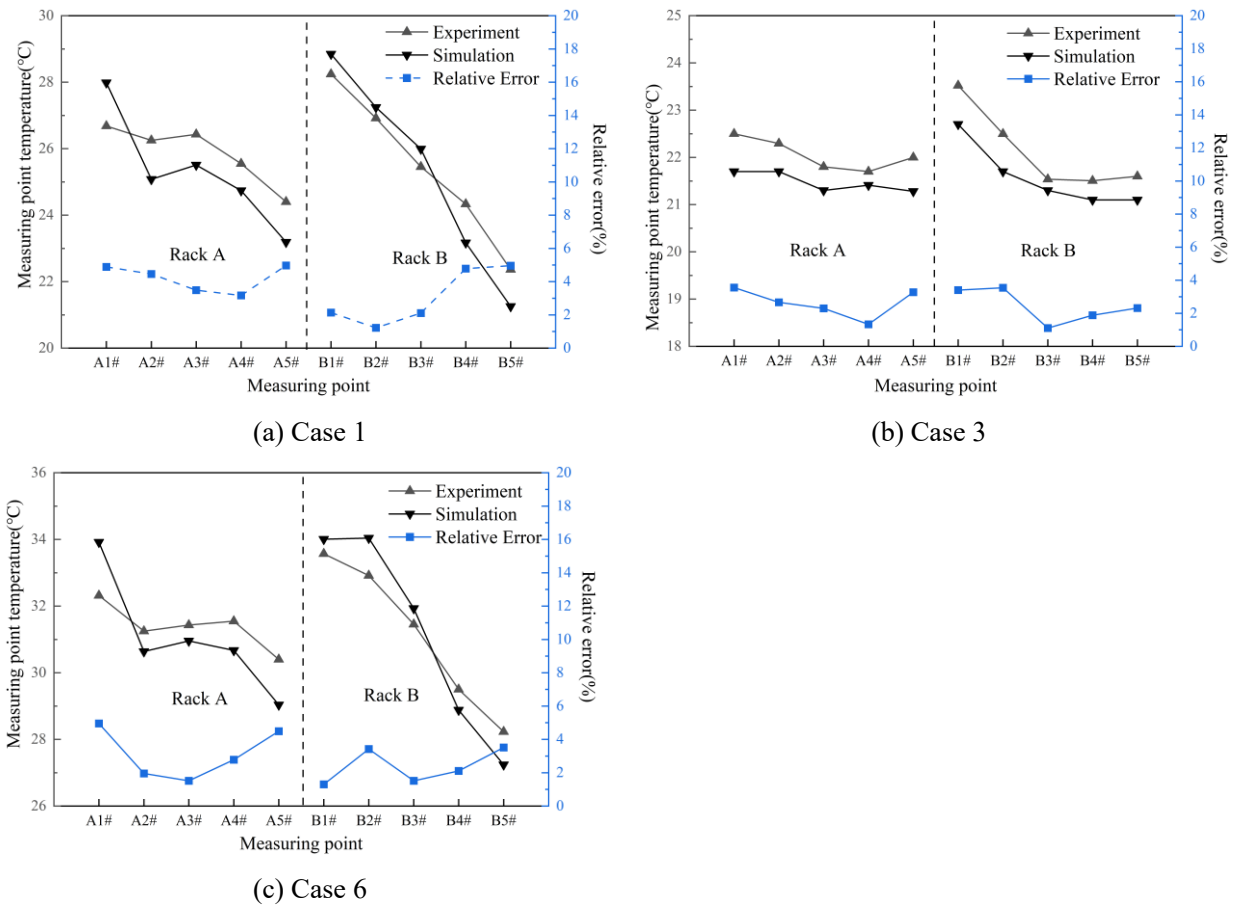

(a) Case 1   (b) Case 3

(c) Case 6

Fig.8. Comparison of experimental and numerical SIAT at measuring points of racks A and B.

It can be found from Fig. 8 that the air temperature of the measuring points from the experiment and simulation has a similar tendency, i.e. the air temperature decreases with the increase of the height of measuring points. At the same measuring point, the temperature difference between the experimental value and the numerical value is -1.6 ~

1.2 °C. The relative error, namely, the ratio of temperature difference to the experimental value, ranges from 1.25% to 5%. It should be noted that, when the SAV is 1 m³/s (case 1 and case 6), at point A1#, the experimental value is significantly less than the numerical value. This could be the reason that point A1# is located at the air inlet of the lowest server in rack A, and on the ground where the rack A is located, more cables are arranged, which hinders some of the hot air return. For the case of 3, when the SAV is increased to 3 m³/s, the return flow of the hot air decreases, leading to a small error. Comparing Fig. 8(a), (b), and (c), the SIAT of rack A and B decreases with the increase of the server height, and the SIAT change of rack B is significantly higher than that of rack A. In general, the numerical results and the experimental results are consistent in the air temperature trend of measuring points, and the deviation between the two is less 5%, indicating the numerical model is valid for the current analysis.

3. Results

3.1 Typical case analysis

In order to discover the temperature control characteristics of the fan-wall DC under ventilation, taking the case with SAV of 1 m³/s, SAT of 21 °C and DCTP of 8 kW as the typical, the air temperature changes at the air inlet and outlet of racks A and B, as well as the airflow around the rack A, were analyzed by a combined experiment and simulation.

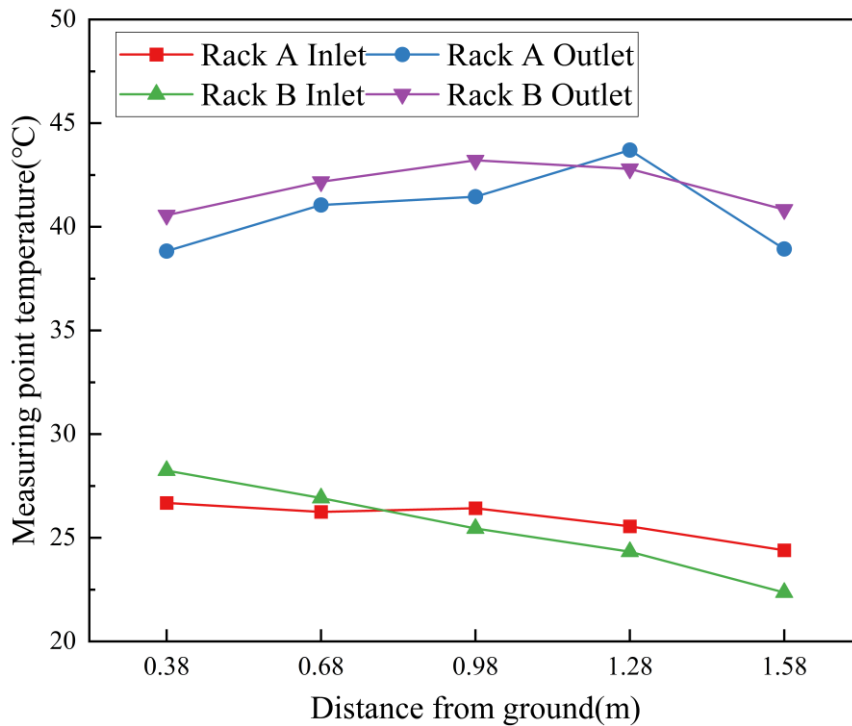### 3.1.1 Air temperature of measuring points

Fig. 9. Air temperature distribution at the air inlet and outlet air of racks A and B.

Fig. 9 plots the air temperature distribution of the measuring points at the air inlet and air outlet of racks A and B, according to the experimental results. It can be observed from Fig. 9 that, on the air inlet side of racks A and B, almost the SIAT at all measuring points is 2 ~ 5 °C higher than that of the SAT. This indicates that the DCTP of the DC affects the supply air temperature and also implies that there may be a return of hot aisle air inside the racks. The SIAT of racks A and B both decrease with the increase of height, it could be explained by the fact tht the higher position of the air supply vent at the fan wall and the return flow of the hot air in the lower part of the racks is less than that in the upper part. Meanwhile, the air temperature difference at the inlet of rack A is smaller than that of rack B, the difference value for the former is about 2 °C but for the latter is about 6 °C, this is due to rack A is closer to

the air supply vent compared to the rack B. In addition, it can be found that, on the air outlet side of racks A and B, the air temperature almost at all measuring points increases with the increase of the height. This is due to the lower density of the hot air could make it move upward. However, it is observed that the air temperature at the point of 1.58 m in height is lower than that at the point of 1.28 m in height. The reason could be in the upper part of the rack, there is an unenclosed area with a height of 0.35 m, from which the cold air can directly enter the hot aisle and mix with the hot air at the measuring point of 1.58 m in height. The temperature difference between the air inlet and outlet of a server increases as the height increases, indicating that the airflow obtained by servers at different heights is not the same. As far as a single rack is concerned, the lower server gets more airflow volume than that of the upper server, this is because that the density of the cold air is larger than that of the hot air, most of the cold air from the air inlet vent will move to the ground. In general, the SIAT is maintained at 25 ± 3 °C, and the outlet air temperature of the servers is maintained at 40 ± 3 °C, which is in agreement with the test results in Ref [45].

3.1.2 Distribution of air temperature field

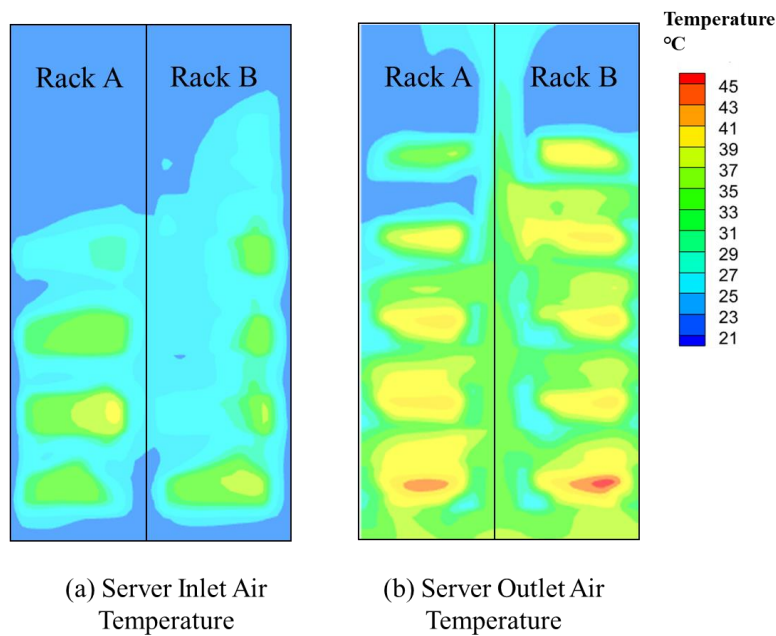(a) Server Inlet Air Temperature (b) Server Outlet Air Temperature

Fig.10. Server inlet and outlet temperature cloud chart.

Fig. 10 numerically shows the contour figures of the air temperature at the air inlet and outlet of racks A and B. It can be found from Fig. 10(a) that, the air temperature at the air inlet of racks A and B both decrease with the increase of the height, which is consistent with the experimental results in Fig. 9. Except for the top area of the rack, the air temperature at the air inlet of racks is significantly higher than that of the SAT. Evenly, the air temperatures in some areas of the air inlet are higher than 27°C, indicating that the operating environment of the server at those location is overheated. As can be seen from Fig. 10(b), the air temperature distribution in the air outlet area of the racks occupied by the servers is relatively uniform as a whole, ranging from 39 °C to 41 °C. Whereas compared to the test results, the air temperature of the bottom server on the outlet side of the rack is significantly higher than the air temperature of the upper server, this could be the reason that the hot air return was neglected in the current numerical simulation. Comparing Fig. 10(a) and Fig. 10(b), it can be observed that, in the upper part of the racks where there is no server, the air temperature at the most area of the air inlet and outlet surfaces has little change, indicating that the cold air flows directly through the rack into the hot aisle, and affects the air temperature at the air outlet of the topmost server. This phenomenon is consistent with the experimental result that, the outlet air temperature at the measuring point of 1.58 m in height is lower than that at the 1.28 m height point.

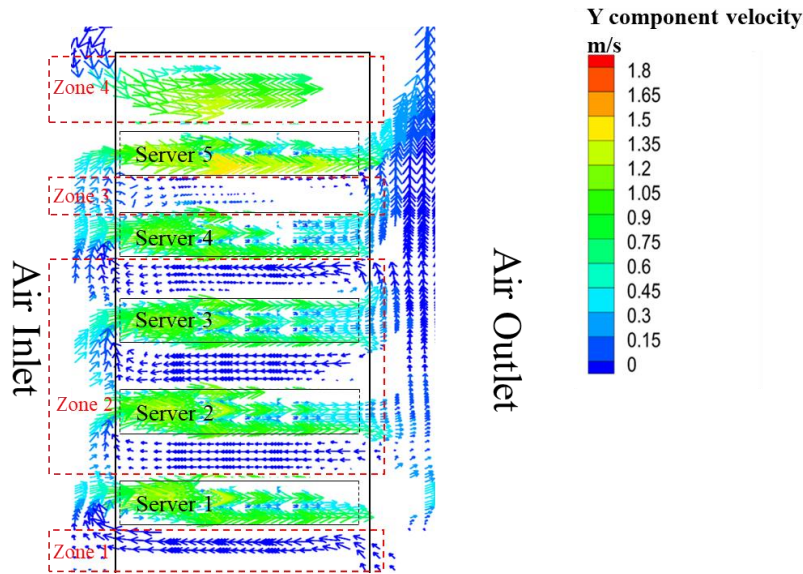### 3.1.3 Distribution of velocity field

Fig.11. Local velocity vector diagram of rack A.

Fig. 11 demonstrates the local velocity vector diagram of rack A based on the numerical result. It can be observed from Fig.11 that the inlet air velocity of the server is 1 ~ 1.5 m/s. Hot air will return from the hot aisle to the cold aisle, with a velocity rate ranging from 0 ~ 0.2 m/s, which leads to an increase in SIAT. Air return velocity can be roughly divided into four zones. The recirculation velocity of hot air in zone 1 is the largest, followed by zone 2 and zone 3. The speed of the return air decreases with the increase of height. Zone 4 not only has no hot air recirculation but also has a cold air bypass.

3.2. Sensitivity analysis
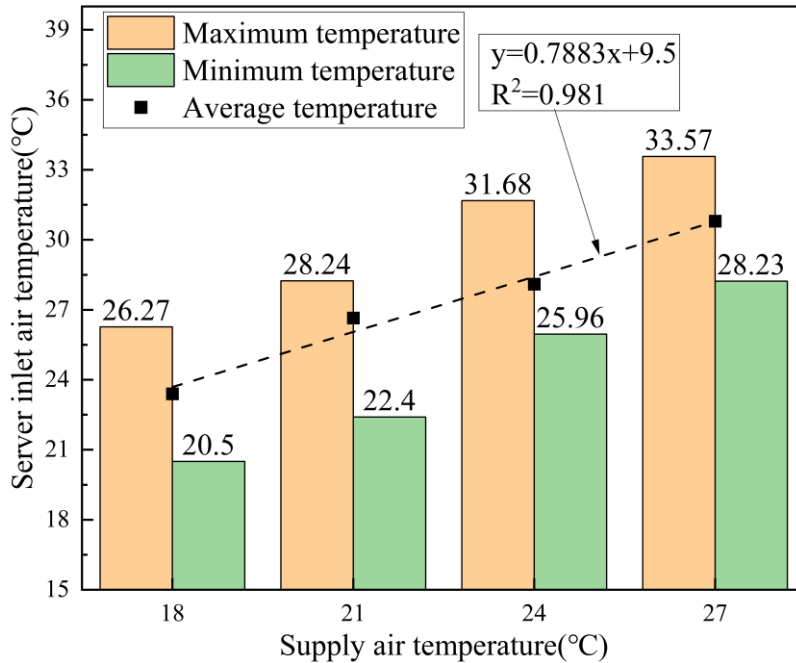
3.2.1. Effect of the SAT

Fig. 12. Maximum, minimum, and average SIAT at different SATs.

Fig.12 plots the maximum, minimum, and average SIAT of the server under different SATs, according to the results of experimental case 1 and cases 4 ~ 6. It can be found from Fig. 12 that, as the SAT increases, the maximum

and minimum SIAT will increase. The average SIAT increases approximately linearly with the SAT. This trend is consistent with the heat load equation of $Q_{ts}=G_m\times c_p\times\varDelta T$, but the slope is 0.7883 instead of 1. This indicates that the return hot air is mixed with cold air at the inlet side of the rack, and the ratio of the cold air to hot air is the same under different SATs. When the SAT is 21 °C, although the average SIAT is less than 27 °C, the maximum air temperature could reach 28.24 °C, indicating that at this SAT, the ambient temperature of some servers is too high. When the SAT is 24 °C, the average SIAT would exceed 27 °C, indicating that with the increase of the SAT, the operating environment of the server will further deteriorate. The temperature difference of the SIAT between the maximum value and the minimum value is relatively stable at 5.34 ~ 5.84 °C, as the change of the SAT, which indicates that the SAT will have a significant linear impact on the operating ambient temperature of the server, but it will not change the uniformity of the SIAT distribution.
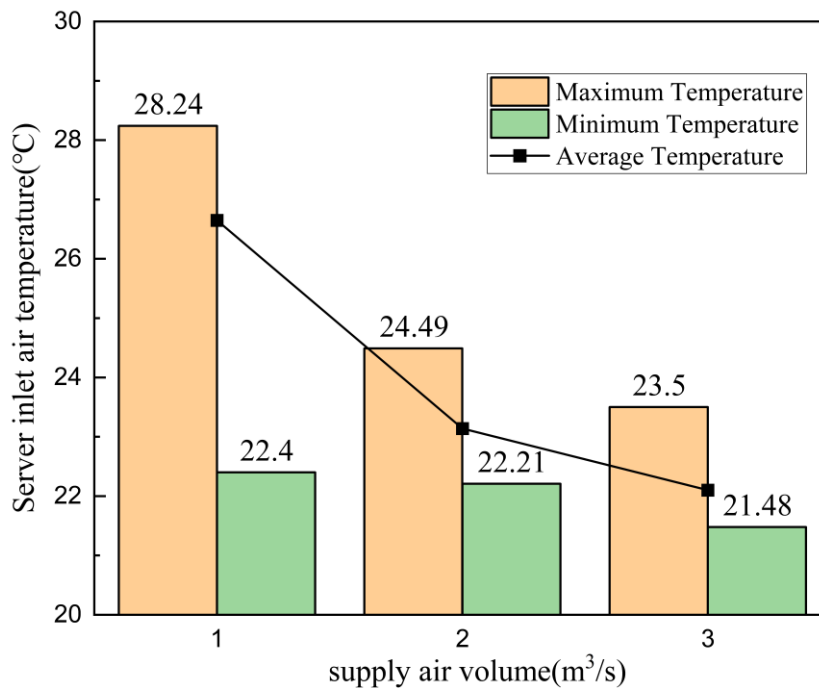
3.2.2. Effect of the SAV

Fig. 13. Maximum, minimum, and average SIAT at different SAVs.

Fig. 13 plots the maximum, minimum, and average SIAT at different SAVs, according to the results of experimental cases 1 ~ 3. It can be found that the average, the maximum, the minimum, and the temperature difference between the maximum and minimum SIAT decrease with the increase in SAV, but there is no significant linear relationship. When the SAV is 1 m³/s, the maximum SIAT is 28.24 °C, exceeding 27 °C. When the SAV increases to 2 m³/s, the maximum SIAT decreases to 24.49 °C. The reason why the SIAT decreases with the SAV is that increasing the SAV reduces the backflow of hot air in the hot aisle and improves the uniformity of the temperature distribution on the front side of the rack.
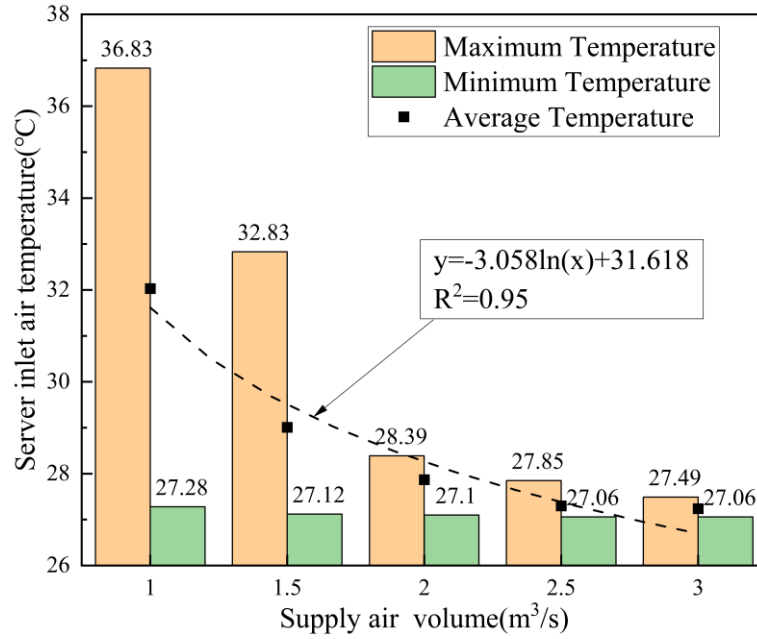
Fig. 14. Maximum, minimum, and average SIAT at different SAVs.

Fig. 14 plots the maximum, minimum, and average SIAT at different SAVs in terms of the results of numerical cases 6 ~ 10. It can be found that the maximum, the average, and the difference between the maximum and minimum SIAT decrease with the increase of SAV, and the minimum SIAT is slightly higher than that of the SAT, which is consistent with the trend shown in Fig. 13, further illustrating the correctness of the simulation model. At the same time, there is a significant logarithmic relationship between the average SIAT and the SAV. When the SAV increases to 2 m³/s, SIAT is slightly higher than that of the SAT, and then increasing the SAV cannot significantly improve the operating environment. It can be deduced that when the SAT is 27 °C, the optimal SAV for the DC is about 2 m³/s, while 0.5 m³/s for a single rack and 0.1 m³/s for a server.
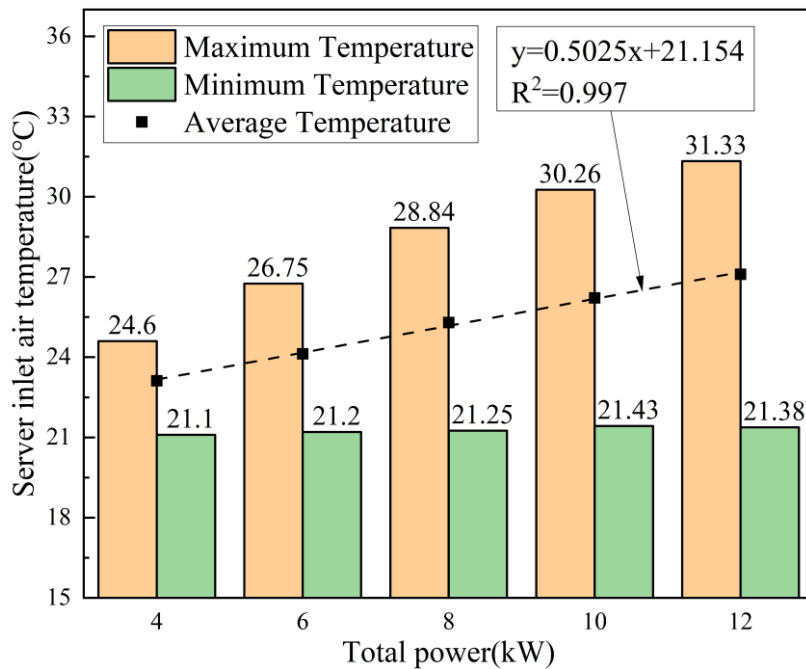
3.2.3. Effect of the DCTP

Fig. 15. Maximum, minimum, and average SIAT at different DCTPs.

Fig. 15 plots the maximum, minimum, and average SIAT at different DCTPs based on the results of numerical

cases 1 ～ 5. It can be found from Fig. 15 that, the maximum SIAT increases with the increase of DCTP, but the minimum SIAT has little change with the DCTP. The average SIAT increases approximately linearly with the DCTP, this is consistent with the law shown by the calorie calculation formula, with a slope of about 0.5025. Under the condition of SAT of 21 °C and SAV of 1 m³/s, when the DCTP is 8 kW, the maximum SIAT exceeds 27 °C, indicating that the operating ambient temperature of some servers is too high. Overall, the increase in the DCTP causes the return air temperature to increase, thereby increasing the air temperature on the front side of the rack.

4. Discussion

From the above results, it can be known that for the fan-wall DC, the DCTP of the rack and supply air parameters play important roles on the temperature control performance. A reliable evaluation method is needed to quantitatively evaluate the server operating environment of the DC. Making the most of natural air is the key to energy savings for fan-wall DCs, but natural air temperatures vary seasonally, so the SAV should also vary with the SAT to ensure thermal safety in the DC. Therefore, it is necessary to obtain a proper ventilation model to protect the thermal environment in fan-wall DCs and minimize the energy consumption of the fans.

4.1. Evaluation of temperature control effect

4.1.1. Evaluating index

At present, there are many evaluation indexes for the thermal environment in DCs, such as rack cooling index (RCI) [46], supply heat index (SHI) [47], β index [31]. The RCI is divided into RCI_{HI} and RCI_{LO}, among them, the RCI_{HI} is a rack cooling index used to evaluate the upper limit of the SIAT based on the maximum allowable SIAT and the maximum recommended SIAT, the value of RCI_{HI} can be calculated as follow [48]

$$RCI_{HI} = 1 - \frac{\sum_{i=1}^{n} (T_x - T_{mr})_{T_x > T_{mr}}}{n \times (T_{ma} - T_{mr})} \qquad (4)$$

where T_x is the average SIAT °C; T_{mr} is the maximum recommended SIAT, °C, usually takes ASHRAE [19] recommended 27 °C; T_{ma} is the maximum allowable SIAT, °C, usually 32 °C; n is the total number of servers.

Usually, the RCI_{HI} value of 100% is optimal for operating servers, it requires that the SAT should not be higher than the recommended SIAT, which reduces the application prospect of air free-cooling technology. According to Gong et al. [47], when the RCI_{HI} value of a DC is greater than 90%, the thermal environment is acceptable for the operating servers. Based on this, the following work will optimize the SAV of the DC under different SAT and DCTP.

4.1.2. Evaluation result

To evaluate the feasibility of the air-side free cooling technology for fan-wall DCs, a series of numerical conditions will be performed, taking into account DCTP of 4 and 12 kW, SAV of 1, 1.5, 2, 2.5 and 3 m³/s, SAT of 15, 18, 21, 24 and 27 °C, respectively. By monitoring the SIAT, the RCI_{HI} value of each condition is calculated by Eq. (4).
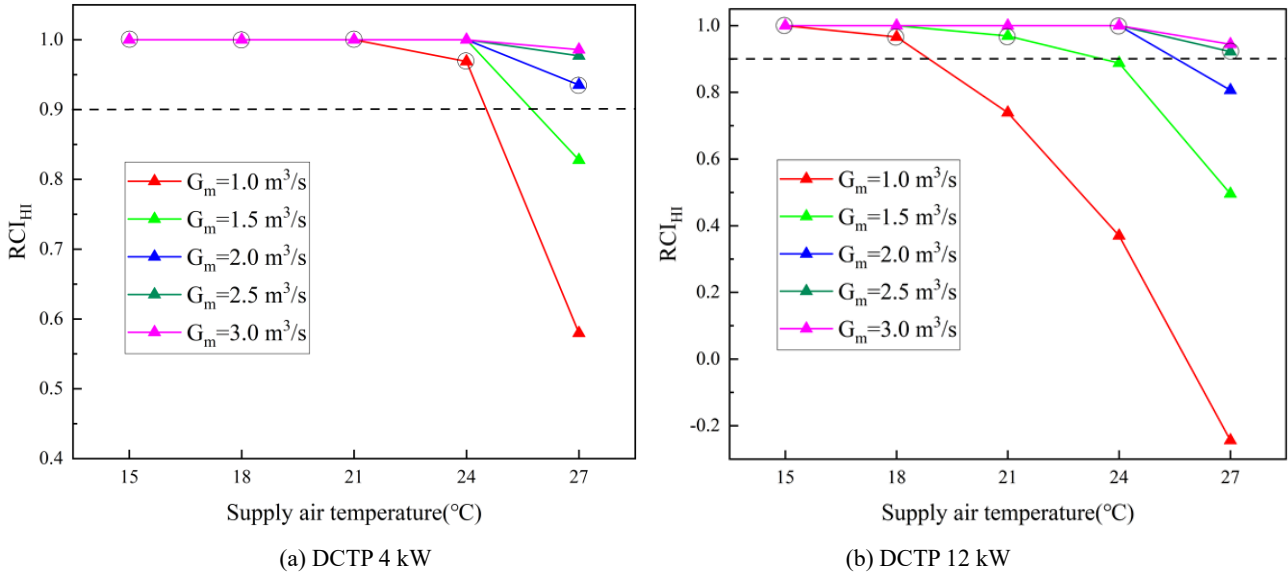
(a) DCTP 4 kW   (b) DCTP 12 kW

Fig. 16. Variation of RCI$_{HI}$ under different supply air conditions.

Fig. 16 (a) and (b) plot the variation of RCI$_{HI}$ under different supply air conditions when the DCTP is 4 kW and 12 kW, respectively. The marked points represent the minimum SAV that satisfies the heat dissipation of the DC. It can be found from Fig. 16(a) that, for the case of DCTP with 4 kW, when the SAT is below 24 °C, the minimum SAV of 1 m³/s can make the RCI$_{HI}$ value larger than 0.9, indicating that the minimum SAV can well meet the heat dissipation of the DC. When the SAT increases to 27 °C, the SAV should be at least 2 m³/s to maintain the RCI$_{HI}$ over 0.9. It can be found from Fig. 16(a) that, for the case of DCTP with 12 kW, when the SAT is less than 18 °C, the minimum SAV of 1 m³/s can make the RCI$_{HI}$ value larger than 0.9. As the SAT increases to 21 °C, the SAV should to be increased to 1.5 m³/s to maintain the RCI$_{HI}$ over 0.9. When the SAT reaches 27 °C, the SAV should be increased to at least 2.5 m³/s.

4.2. Establishment of ventilation model

To obtain an appropriate ventilation model, the minimum SAV for the DC with RCI$_{HI}$ value greater than 0.9 under different SATs is selected, when the DCTP values are 4 kW and 12 kW, respectively, and the relationships between the SAV and the SAT are obtained. On this basis, an empirical SAV model under different DCTP is proposed for the fan-wall DC.
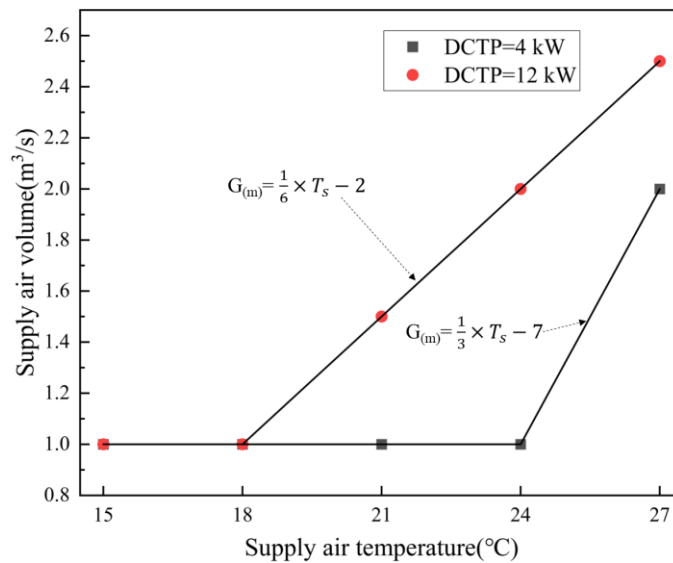

Fig. 17. The SAV curve at different SAT in the DCTP 4 kW and 12 kW.

Fig. 17 plots the curves of the SAV that meet the cooling requirements of the DC under different SATs when the DCTP is 4 kW and 12 kW, respectively. According to Fig. 17, the curve is divided into two sections. In the case of a DCTP of 4 KW, when the SAT does not exceed 24 °C, the minimum SAV of 1 m³/s can meet the cooling requirements. As the SAT rises, the SAV will increase linearly and the slope is 1/3. In the case of a DCTP of 12 KW, when the SAT does not exceed 18 °C, the minimum SAV of 1 m³/s can meet the cooling requirements. After that, the SAV will linearly increase with the SAT, accompanied by a slope of 1/6. This means that for the fan-wall DC, there is a linear relationship between the SAV and SAT, and its slope and intercept are related to the DCTP. Therefore, the calculation of the SAV can be assumed as follow.

$$G_m = F_1(Q_{ts}) \times T_s + F_2(Q_{ts}) \tag{5}$$

where, $F_1(Q_{ts})$ and $F_2(Q_{ts})$ are functions of DCTP.

According to the conservation of energy theory, in a fan-wall DC, the relationship between the SAV and the DCTP can be expressed as follow.

$$G_m = \frac{Q_{ts}}{c_p \times \Delta T} \tag{6}$$

where, ΔT is the DC inlet and outlet air temperature difference; G_m is SAV; Q_{ts} is DCTP.

The change in the specific heat capacity of the air at constant pressure is negligible, therefore the SAV required by the DC is approximately proportional to the DCTP, according to Eq. (6). Thus, the relationship between the SAV required for DC cooling and the SAT and DCTP can be further expressed as follow.

$$G_{(m,ts)} = (A_{1,i} \times Q_{ts} + B_{1,i}) \times T_s + (A_{2,i} \times Q_{ts} + B_{2,i}) \tag{7}$$

where, $G_{(m,ts)}$ is SAV; T_s is SAT; $A_{1,i}, A_{2,i}, B_{1,i}, B_{2,i}$ are constants.

The DCTP for a DC is not static, it is related to the SIAT and server memory usage [49]. Currently, there is no clear and reliable model to predict the changing power of a server [50]. Therefore, in the current work, the DCTP is assumed to range from 4 kW to 12 kW. The SAV models for the DC with DCTP of 4 kW and 12 kW are $G_m=T_s/3-7$ and $G_m=T_s/6-2$, respectively, as shown in Fig.17. Thus, $A_{1,i}, A_{2,i}, B_{1,i}$, and $B_{2,i}$ in Eq. (7) can be obtained by the undetermined coefficient method. The optimal SAV to meet the heat dissipation of the DC under different DCTP is listed as follows.

$$G_{(m,ts)} = \begin{cases} 1 & T_s < 18\ ^\circ\text{C} \\ (\frac{1}{48} \times Q_{ts} - \frac{1}{12}) \times T_s + (-\frac{3}{8} \times Q_{ts} + \frac{5}{2}) & 18\ ^\circ\text{C} \le T_s < 24\ ^\circ\text{C} \\ (-\frac{1}{48} \times Q_{ts} + \frac{5}{12}) \times T_s + (\frac{5}{8} \times Q_{ts} - \frac{19}{2}) & 24\ ^\circ\text{C} \le T_s < 27\ ^\circ\text{C} \end{cases} \tag{8}$$

According to Eq. (8), when the SAT is less than 18 °C, the minimum SAV of the DC is 1 m³/s. When the SAT exceeds 18 °C, the SAV is determined by the DCTP and the SAT. It should be noted here that Eq. (8) only applies when the DCTP varies from 4 kW to 12 kW and the SAT varies from 15 °C to 27 °C.

4.3. Verification of the ventilation model

To verify the applicability of the proposed SAV model, SAV for conditions with DCTP of 6, 8, 10 kW and SAT of 15, 18, 21, 24 and 27 °C, are calculated according to Eq. (8), respectively. After that, the corresponding DCTP, SAT, and SAV values are taken into the numerical analysis to obtain the SIAT of each condition. Finally, the RCI$_{HI}$ value of each condition is calculated by Eq. (4).
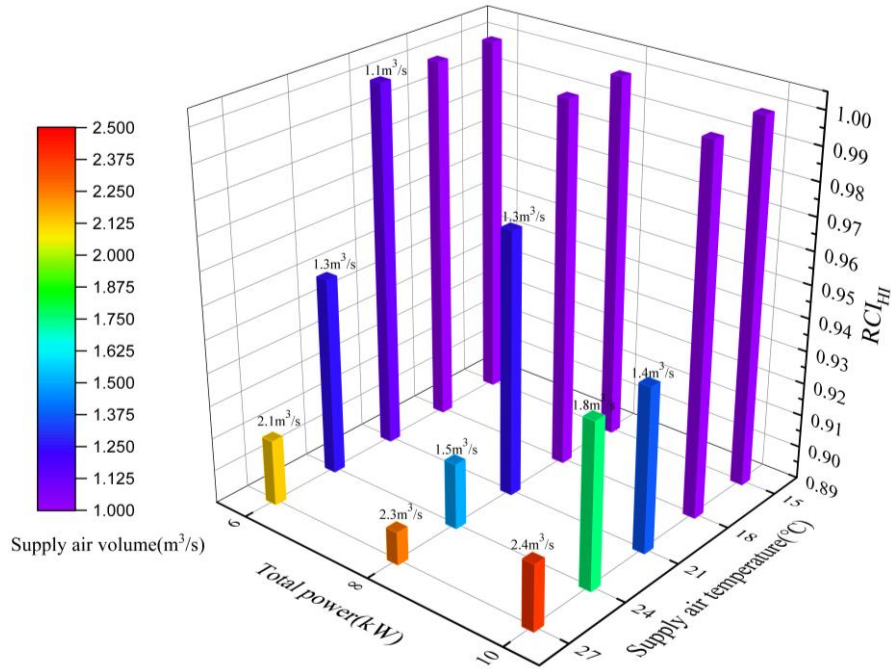
Fig. 18. RCI$_{HI}$ values of DC under different ventilation when the DCTP is 6 kW, 8 kW, and 10 kW.

Fig. 18 shows the RCI$_{HI}$ values of the DC under different ventilation when the DCTP is 6, 8 and 10 kW, respectively. It can be found that, in the case of three different DCTPs, when the SAT is less than 18 °C and the SAV is 1 m^3/s, the RCI$_{HI}$ is equal to 1. When the SAT is over 18 °C, although the RCI$_{HI}$ decreases with the increase of the SAT, its value is larger than 0.9, which indicates that Eq. (8) can well meet the DC heat dissipation.

4.4. Energy-saving prospects for the ventilation model

When the DCTP is 10 Kw in the test DC, the SAV calculated by Eq. (8) is 2.4 m^3/s, which increases the energy consumption of fans by 20%, compared to the SAV of 2 m^3/s, but it reduces the probability of server downtime caused by high temperatures in DC. When the SAT is below 27 °C, the SAV of 2 m^3/s does not significantly increase the reliability of server operation but means more energy consumption due to the high speed of fans. Compared with DC using a constant SAV of 2 m^3/s, the SAV optimized by Eq. (8) for the DC can reduce the energy consumption of fans by 50%, 35%, and 10%, respectively, when the SAT is below 18, 21 and 24 °C. Therefore, optimizing the SAV of DC located in mild climate regions can significantly reduce ventilation system energy consumption.

Guiyang, Guizhou Province, China, is a typically mild climate region, where the outdoor temperature below 18 °C, 18 °C ~ 21 °C, 21 °C ~ 24 °C, 24 °C ~ 27 °C and exceeding 27 °C accounts for 58%, 15%, 16%, 8% and 3% during a whole one year, respectively. As far as a fan-wall DC is concerned, the SAV optimized by Eq. (8) can reduce the energy consumption of the fan by 34% in one year, compared to a constant SAV.

5. Conclusions

In this study, the influence of the SAV and SAT on the temperature control performance of a DC is tested by the self-built DC test rig, and the DC ambient temperature distribution characteristics are obtained. On this basis, the full-scale numerical model is established and validated against experimental results. The influence of air supply parameters and DCTP is further explored through numerical analysis, and get the optimal SAV under the extreme SAT. The main conclusions are summarized as follows:

(1) Due to the hot air backflow, the SIAT is higher than the SAT, and the SIAT decreases with the increase in rack height.

(2) The increase in DCTP reduces the uniformity of the SIAT distribution, yet the increase in SAT hardly change the uniformity of SIAT distribution.

(3) The average SIAT increases logarithmically with the SAV, when the SAV reaches a certain limit, increasing the SAV cannot significantly improve the thermal environment of the DC. When the SAT is 27 °C, the optimal SAV for a single rack with a power of 2.5 kW is approximately 0.5 m^3/s.

(4) To ensure the thermal safety of fan-wall DCs, an empirical SAV model is proposed and verified through more numerical cases.

(5) This empirical ventilation model can reduce the annual energy consumption of fans by 34% for fan-wall DCs located in Guiyang.

The SAV model of experience may change with different cooling arrangements, and exploring the impact of different cooling arrangements on DC heat dissipation performance will be one of our future work directions. In addition, in future work, we will deeply explore the change rule of the server power with the SIAT and server occupancy, and there are some issues worth further discussion about the temperature control of the fan wall DC. For example, the structural parameters of the DC are optimized to improve the cooling efficiency.

Declaration of competing interest

The authors declare that they have no known competing financial interests or personal relationships that could have appeared to influence the work reported in this paper.

Acknowledgments

References

[1] Y. Xu, R. Liu, L. Tang, H. Wu, C. She, Risk-averse multi-objective optimization of multi-energy microgrids integrated with power-to-hydrogen technology, electric vehicles and data center under a hybrid robust-stochastic technique, Sustain Cities Soc. 79 (2022) 103699, https://doi.org/10.1016/j.scs.2022.103699.

[2] Y. Ichinose, M. Hayashi, S. Nomura, B. Moser, K. Hiekata, Sustainable Data Centers in Southeast Asia: Offshore, Nearshore, and Onshore Systems for Integrated Data and Power, Sustain Cities Soc. 81 (2022) 103867, https://doi.org/10.1016/j.scs.2022.103867.

[3] X. Shao, Z. Zhang, P. Song, Y. Feng, X. Wang, A review of energy efficiency evaluation metrics for data centers, Energ Buildings. 271 (2022) 112308, https://doi.org/10.1016/j.enbuild.2022.112308.

[4] C.M. Tan, G. Zhang, Overcoming intrinsic weakness of ULSI metallization electromigration performances, Thin Solid Films. 462-463 (2004) 263-268, https://doi.org/10.1016/j.tsf.2004.05.054.

[5] E. Masanet, A. Shehabi, N. Lei, S. Smith, J. Koomey, Recalibrating global data center energy-use estimates, Science. 367 (6481) (2020), https://www.science.org/doi/10.1126/science.aba3758.

[6] E. Oró, P. Taddeo, J. Salom, Waste heat recovery from urban air cooled data centres to increase energy efficiency of district heating networks, Sustain Cities Soc. 45 (2019) 522-542, https://doi.org/10.1016/j.scs.2018.12.012.

[7] S. Lim, H. Chang, Airflow management analysis to suppress data center hot spots, Build Environ. 197 (2021) 107843, https://doi.org/10.1016/j.buildenv.2021.107843.

[8] J. Wang, Z. Huang, Z. Liu, C. Yue, P. Wang, S. Yoon, In-situ sensor correction method for data center cooling systems using Bayesian Inference coupling with autoencoder, Sustain Cities Soc. 76 (2022) 103514, https://doi.org/10.1016/j.scs.2021.103514.

[9] Y. Zhang, K. Shan, X. Li, H. Li, S. Wang, Research and Technologies for next-generation high-temperature data centers – State-of-the-arts and future perspectives, Renew Sust Energ Rev. 171 (2023) 112991, https://doi.org/10.1016/j.rser.2022.112991.

[10] M. Borkowski, A.K. Piłat, Customized data center cooling system operating at significant outdoor temperature fluctuations, Appl Energ. 306 (2022) 117975, https://doi.org/10.1016/j.apenergy.2021.117975.

[11] E.A. Amado, P.S. Schneider, C.S. Bresolin, Free cooling potential for Brazilian data centers based on approach point methodology, Int J Refrig. 122 (2021) 171-180, https://doi.org/10.1016/j.ijrefrig.2020.11.010.

[12] Y. Gong, F. Zhou, G. Ma, S. Liu, Advancements on mechanically driven two-phase cooling loop systems for data center free cooling, Int J Refrig. 138 (2022) 84-96, https://doi.org/10.1016/j.ijrefrig.2022.03.007.

[13] C. Nadjahi, H. Louahlia, S. Lemasson, A review of thermal management and innovative cooling strategies for data center, Sustainable Computing: Informatics and Systems. 19 (2018) 14-28, https://doi.org/10.1016/j.suscom.2018.05.002.

[14] X. Han, W. Tian, J. VanGilder, W. Zuo, C. Faulkner, An open source fast fluid dynamics model for data center thermal management, Energy Build. 230 (2021) 110599, https://doi.org/10.1016/j.enbuild.2020.110599.

[15] E. Oró, V. Depoorter, N. Pflugradt, J. Salom, Overview of direct air free cooling and thermal energy storage potential energy savings in data centres, Appl Therm Eng. 85 (2015) 100-110, https://doi.org/10.1016/j.applthermaleng.2015.03.001.

[16] M. Deymi-Dashtebayaz, S. Valipour Namanlo, A. Arabkoohsar, Simultaneous use of air-side and water-side economizers with the air source heat pump in a data center for cooling and heating production, Appl Therm Eng. 161 (2019) 114133, https://doi.org/10.1016/j.applthermaleng.2019.114133.

[17] M. Deymi-Dashtebayaz, S.V. Namanlo, Potentiometric and economic analysis of using air and water-side economizers for data center cooling based on various weather conditions, Int J Refrig. 99 (2019) 213-225, https://doi.org/10.1016/j.ijrefrig.2019.01.011.

[18] K. Lee, H. Chen, Analysis of energy saving potential of air-side free cooling for data centers in worldwide climate zones, Energ Buildings. 64 (2013) 103-112, https://doi.org/10.1016/j.enbuild.2013.04.013.

[19] ASHRAE, Equipment Thermal Guidelines for Data Processing Environments, ed. Technical Committee (TC) 9.9, 2021.

[20] V.E. Ahmadi, H.S. Erden, A parametric CFD study of computer room air handling bypass in air-cooled data centers, Appl Therm Eng. 166 (2020) 114685, https://doi.org/10.1016/j.applthermaleng.2019.114685.

[21] J. Cho, J. Woo, Development and experimental study of an independent row-based cooling system for improving thermal performance of a data center, Appl Therm Eng. 169 (2020) 114857, https://doi.org/10.1016/j.applthermaleng.2019.114857.

[22] J. Cho, B. Park, S. Jang, Development of an independent modular air containment system for high-density data centers: Experimental investigation of row-based cooling performance and PUE, Energy. 258 (2022) 124787, https://doi.org/10.1016/j.energy.2022.124787.

[23] H. Moazamigoodarzi, P.J. Tsai, S. Pal, S. Ghosh, I.K. Puri, Influence of cooling architecture on data center power consumption, Energy. 183 (2019) 525-535, https://doi.org/10.1016/j.energy.2019.06.140.

[24] Y. Zhang, K. Zhang, J. Liu, R. Kosonen, X. Yuan, Airflow uniformity optimization for modular data center based on the constructal T-shaped underfloor air ducts, Appl Therm Eng. 155 (2019) 489-500, https://doi.org/10.1016/j.applthermaleng.2019.04.025.

[25] X. Yuan, X. Xu, J. Liu, Y. Pan, R. Kosonen, Y. Gao, Improvement in airflow and temperature distribution with an in-rack UFAD system at a high-density data center, Build Environ. 168 (2020) 106495, https://doi.org/10.1016/j.buildenv.2019.106495.

[26] X. Yuan, Y. Wang, J. Liu, X. Xu, X. Yuan, Experimental and numerical study of airflow distribution optimisation in high-density data centre with flexible baffles, Build Environ. 140 (2018) 128-139, https://doi.org/10.1016/j.buildenv.2018.05.043.

[27] X. Yuan, X. Zhou, J. Liu, Y. Wang, Risto Kosonen, X. Xu, Experimental and numerical investigation of an airflow management system in data center with lower-side terminal baffles for servers, Build Environ. 155 (2019) 308-319, https://doi.org/10.1016/j.buildenv.2019.03.039.

[28] P. Song, Z. Zhang, Y. Zhu, Numerical and experimental investigation of thermal performance in data center with different deflectors for cold aisle containment, Build Environ. 200 (2021) 107961, https://doi.org/10.1016/j.buildenv.2021.107961.

[29] C. Jin, X. Bai, The study of servers' arrangement and air distribution strategy under partial load in data centers, Sustain Cities Soc. 49 (2019) 101617, https://doi.org/10.1016/j.scs.2019.101617.

[30] A.M. Abbas, A.S. Huzayyin, T.A. Mouneer, S.A. Nada, Thermal management and performance enhancement of data centers architectures using aligned/staggered in-row cooling arrangements, Case Stud Therm Eng. 24 (2021) 100884,

https://doi.org/10.1016/j.csite.2021.100884.

[31] S.A. Nada, A.M. Abbas, Solutions of thermal management problems for terminal racks of in-row cooling architectures in data centers, Build Environ. 201 (2021) 107991, https://doi.org/10.1016/j.buildenv.2021.107991.

[32] C. Jin, X. Bai, Y. An, J. Ni, J. Shen, Case study regarding the thermal environment and energy efficiency of raised-floor and row-based cooling, Build Environ. 182 (2020) 107110, https://doi.org/10.1016/j.buildenv.2020.107110.

[33] Y. Lee, C. Wen, Y. Shih, Z. Li, A. Yang, Numerical and experimental investigations on thermal management for data center with cold aisle containment configuration, Appl Energ. 307 (2022) 118213, https://doi.org/10.1016/j.apenergy.2021.118213.

[34] W. Chu, C. Wang, A review on airflow management in data centers, Appl Energ. 240 (2019) 84-119, https://doi.org/10.1016/j.apenergy.2019.02.041.

[35] M.I. Tradat, Y.M.A. Manaserh, B.G. Sammakia, C.H. Hoang, H.A. Alissa, An experimental and numerical investigation of novel solution for energy management enhancement in data centers using underfloor plenum porous obstructions, Appl Energ. 289 (2021) 116663, https://doi.org/10.1016/j.apenergy.2021.116663.

[36] M. Tatchell-Evans, N. Kapur, J. Summers, H. Thompson, D. Oldham, An experimental and theoretical investigation of the extent of bypass air within data centres employing aisle containment, and its impact on power consumption, Appl Energ. 186 (2017) 457-469, https://doi.org/10.1016/j.apenergy.2016.03.076.

[37] Y. Fulpagare, P. Hsu, C. Wang, Experimental analysis of airflow uniformity and energy consumption in data centers, Appl Therm Eng. 209 (2022) 118302, https://doi.org/10.1016/j.applthermaleng.2022.118302.

[38] H. Lu, Z. Zhang, L. Yang, A review on airflow distribution and management in data center, Energ Buildings. 179 (2018) 264-277, https://doi.org/10.1016/j.enbuild.2018.08.050.

[39] M. Kuzay, A. Dogan, S. Yilmaz, O. Herkiloglu, A.S. Atalay, A. Cemberci, C. Yilmaz, E. Demirel, Retrofitting of an air-cooled data center for energy efficiency, Case Stud Therm. Eng. 36 (2022) 102228, https://doi.org/10.1016/j.csite.2022.102228.

[40] X. Xiong, Y. Fulpagare, P.S. Lee, A numerical investigation of fan wall cooling system for modular air-cooled data center, Build Environ. 205 (2021) 108287, https://doi.org/10.1016/j.buildenv.2021.108287.

[41] X. Xiong, P.S. Lee, Vortex-enhanced thermal environment for air-cooled data center: An experimental and numerical study, Energ Buildings. 250 (2021) 111287, https://doi.org/10.1016/j.enbuild.2021.111287.

[42] X. Meng, J. Zhou, X. Zhang, Z. Luo, H. Gong, T. Gan, Optimization of the thermal environment of a small-scale data center in China, Energy. 196 (2020) 117080, https://doi.org/10.1016/j.energy.2020.117080.

[43] P.H. Guo, S. Wang, Y.Q. Lei, J.Y. Li, Numerical simulation of solar chimney-based direct airside free cooling system for green data centers, J Build Eng. 32 (2020), https://doi.org/10.1016/j.jobe.2020.101793.

[44] C. Jin, X. Bai, C. Yang, Effects of airflow on the thermal environment and energy efficiency in raised-floor data centers: A review, Sci Total Environ. 695 (2019) 133801, https://doi.org/10.1016/j.scitotenv.2019.133801.

[45] Y. Fulpagare, P.H. Hsu, C.C. Wang, Experimental analysis of airflow uniformity and energy consumption in data centers, Appl Therm Eng. 209 (2022), https://doi.org/10.1016/j.applthermaleng.2022.118302.

[46] C. Wang, Y. Tsui, C. Wang, On cold-aisle containment of a container datacenter, Appl. Therm. Eng. 112 (2017) 133-142, https://doi.org/10.1016/j.applthermaleng.2016.10.089.

[47] X. Gong, Z. Zhang, S. Gan, B. Niu, L. Yang, H. Xu, M. Gao, A review on evaluation metrics of thermal performance in data centers, Build. Environ. 177 (2020) 106907, https://doi.org/10.1016/j.buildenv.2020.106907.

[48] M.K. Herrlin, Rack Cooling Effectiveness in Data Centers and Telecom Central Offices: The Rack Cooling Index (RCI), AHRAE Trans. 111 (2005) 725-731.

[49] C. Jin, X. Bai, X. Zhang, X. Xu, Y. Tang, C. Zeng, A measurement-based power consumption model of a server by considering inlet air temperature, Energy. 261 (2022) 125126, https://doi.org/10.1016/j.energy.2022.125126.

[50] C. Jin, X. Bai, C. Yang, W. Mao, X. Xu, A review of power consumption models of servers in data centers, Appl Energ. 265 (2020) 114806, https://doi.org/10.1016/j.apenergy.2020.114806.